Progress In Electromagnetics Research B, Vol. 53, 291–314, 2013

FAULT PREDICTION OF DEEP BAR CAGE ROTOR INDUCTION MOTOR BASED ON FEM

Basil Saied[1] and Ahmed Ali[2, *]

[1]Electrical Engineering Department, University of Mosul, Iraq

[2]Foundation of Technical Education, Technical College of Engineering, Mosul, Iraq

Abstract—The paper aims to investigate the use of the Finite Element Method for electrical and mechanical faults detection in three-phase squirrel cage, induction machines. The features of Finite Element Method are significant, which consider the physical mapping of stator winding and rotor bar distribution. Therefore, modeling of the faults in stator winding, rotor bars and air-gap eccentricity will be predicated in more accurate way. In comparison with conventional methods such as coupling method, the Finite Element Method considers the complex machine geometry, material type of the bar, current and the flux distributions within the electrical machines. As a result, the air-gap eccentricity and the broken bars can be modeled effectively using this approach. Motor current signature analysis has been used to give a decision about the fault occurrence. For the broken rotor bar, frequency of the sideband components around the fundamental is used to indicate the presence of fault. However, the sideband frequencies cannot be used to recognize the stator winding short circuit and eccentricities faults, where the harmonics have approximately the same frequency over the spectrum. The amplitude of the sideband harmonic components have been used to differentiate between them. It has been found that the inter-turn short circuit faults have a sideband harmonic component with amplitude greater than that in the case of the air-gap eccentricity faults. Also current paper introduces the detection of broken rotor bars based on stator current envelope technique.

Received 19 June 2013, Accepted 30 July 2013, Scheduled 6 August 2013

* Corresponding author: Ahmed Ali (ahmedem71@gmail.com).

1. INTRODUCTION

Three-phase cage rotor, induction machines have wide spreading on industrial applications due to their low cost and maintenance requirements, ability to work in polluted environments and rigidity. The electrical machine has to be monitored so that faults can be predicted as early as possible, and consequently the machine and its function can be protected. Mechanical and electrical faults can occur in this type of machines; the mechanical faults represent about 50% of the faults [1, 2]. Bearing is one of the most occurring mechanical faults. In advance stage, it will cause severe air-gap eccentricity [3]. The electrical faults can take place on both stator and rotor. The main types of these faults are inter-turn short circuit of stator winding, which represents about 30%, and broken bar, which represents about 10%. Finally, 10% of the faults represent external faults [4]. The main types of the electric machines faults are detected by analyzing the stator current [5, 6]. For all faults eccentricity types, two parameters are considered to indicate the type of faults, which are the frequency and amplitude of the harmonics in the spectrum of the stator current. The classical methods had been used to determine the frequency of the sideband harmonics correctly. Due to approximation criteria used in these methods, the amplitude of the sideband harmonics has a considerable deviation from the experimental methods [7, 8].

Numerical methods were used to determine the parameters of electrical machines such as magnetic coupling method and winding and extended winding function methods that give more accurate results than analytical approach. Complex geometry, non-linear behavior of core materials and actual representation of winding distribution on the stator slots can be efficiently modeled using FEM. This will provide an accurate calculation of electromagnetic fields and as a consequence all the machine parameters. FEM is used to determine the linear or non-linear behaviors of electromagnetic fields by solving a set of Maxwell's equations. In this paper, a two-dimensional model is considered to construct the geometry of three-phase cage-type induction motor based on finite element transient analysis.

The operation of three-phase induction motor using transit finite element analysis was considered. The motor current signature analysis (MCSA) was employed to detect the mixed air-gap eccentricity [1]. The static and dynamic eccentricities were simulated using time stepping finite element method (TSFEM). These types of faults were detected based on the amplitude of sideband harmonics components around fundamental component and principle slot harmonic (PSH). It was proven that the amplitude of sideband components around

the fundamental harmonic could be used as a factor to detect the fault occurrence without its type, while the amplitude of the sideband harmonics components on PSH and around it can be used to detect the air-gap eccentricity fault and its type [2]. A 2-D FEM was used to simulate and analyze the performance of electric machine. Solution of electromagnetic filed equations provides acceptable information about healthy and inter-turn short circuit. The winding in each phase was divided into different groups in order to model the different types of short circuit fault. The coils of stator phases are divided into two parts connected in series with equal turns for each part. By this method, a short circuit can be implemented at any location of the coil [5]. FEM considers a powerful tool used to model and study different type of broken rotor bars. It was found that this type of faults changes the distribution of the losses on stator core and the distribution of the current on the rotor circuit. In addition, the rotor bars circuit is subjected to the thermal effect in case of adjacent broken rotor bars [6]. In the case of inter-turn stator winding fault, the distribution of magnetic field parameters was distorted, and the stored energy is reduced when the severity of winding increases [9]. Magneto-static analysis based on finite element analysis is used to determine the variation of the flux and stored energy in the electric machines [9, 10]. Based on this type of analysis, the variation of the magnetic flux, magnetic flux density and stored energy can be computed accurately. A complete model of a cage-rotor three-phase squirrel induction motor was modeled using MagNet. Due to the broken bars, the distribution of the magnetic force on the slot teeth near the broken bars was reduced. In addition, increasing the number of broken bars leads to reduce the stored magnetic energy [10].

In the current paper, FEM has been used to simulate and detect the main types of faults in three-phase squirrel cage induction machines. FEM is used to build the complex geometry of the model, and the type of materials is selected to specify the stator windings, rotor bars and iron cores. As a result, all electrical and mechanical faults types can be modeled smoothly based on this numerical method. MCSA has been used to give a decision about the fault occurrence. In case of broken rotor bar, the sideband frequency components around the fundamental give indication about the attendance of fault. Additionally, a detection of broken rotor bars based on stator current envelope technique has been introduced. In case of the air-gap eccentricity and stator winding short circuit faults, the harmonics have approximately the same sidebands components over the spectrum. It has been found that the inter-turn short circuit faults have a sideband harmonic component at $k = 4$ with amplitude greater than that in

the case of the air-gap eccentricity faults. This factor can be used to recognize between these types of faults.

2. TYPES OF INDUCTION MOTOR FAULTS

In the current paper, the following common types of induction machines faults are presented.

2.1. Broken Rotor Bar Faults

These common faults occur on the movement part of cage rotor type or synchronous machine, which has damper bars. Cracking or breaking these bars arises due to manufacturing problem on the bar itself or due to high value of bar currents which induce through rotor circuits. These currents are caused by unbalanced, sudden or over loading of the machine. It had been shown that the broken bar may affect the material properties of the core and the current distribution of the adjacent rotor bars. Therefore, the adjacent bar is more susceptible to break than the nonadjacent bar.

2.2. Stator Winding Faults

In this type of faults, a short circuit could occur between two adjacent turns, coils or even between phases. In advanced stage, faults may take place between the core and the stator windings. Harmonics components of the flux density in the air-gap region may be used to give an indication about the stator turn faults. As a result, the magnetic flux as well as flux density will be deformed, and stored magnetic energy will decrease in proportion to the degree of short circuit [9]. Therefore, it is possible to diagnose the faults of induction machines by analyzing the magnetic field quantities.

2.3. Air-gap Eccentricity Faults

In this kind of faults, the air-gap of the machine has unequal spaces along the outer radius of rotor. Air-gap eccentricity faults may occur due to damage of the mechanical parts of the electric machine like the gearbox bearings. These misalignments of the shaft include static eccentricity, dynamic eccentricity or mixed eccentricity. In static eccentricity, although the axial axis of the rotor coincides with the axial axis of rotation, it does not coincide with stator axis, and the minimum air-gap position is fixed. In dynamic eccentricity, the rotor axial axis does not coincide with the axis of rotation, and the minimum air-gap position rotates along the internal boundary of the stator.

In mixed eccentricity, both the stator and rotor axial axes coincide between the two axes of rotations. The frequencies of the harmonics around the fundamental component give good indication that there is an eccentricity fault type, while the amplitude of the sideband harmonics around the PSH indicates the type of eccentricity.

3. FAULT ANALYSIS TECHNIQUES

3.1. Park Method (PM)

In this technique, three-phase stator currents is transformed into two-phase system using the following equations:

$$i_\alpha = \sqrt{\frac{2}{3}} i_A - \sqrt{\frac{1}{6}} i_B - \sqrt{\frac{1}{6}} i_C \tag{1}$$

$$i_\beta = \sqrt{\frac{1}{2}} i_B - \sqrt{\frac{1}{2}} i_C \tag{2}$$

In the normal case of machine operation, without fault, the relation between the two currents in the Eqs. (1) and (2) have approximately a circle shape centered at the origin. For the abnormal operating conditions (such as single phasing, short circuit of stator winding, broken bars or air-gap eccentricity), the three-phase stator currents become unbalanced, which produce an oscillation in the radius of the Park vector, by substituting the instantaneous values of three-phase stator currents in Eqs. (1) and (2). Therefore, the trajectory deviates from circle to elliptic form [1]. The degree of deviation and the axial angle of the elliptic locus depend on the severity degree and type of the faults.

3.2. Fast Fourier Transform Method

This method is adopted in the present paper to analyze the stator current. Then the frequency spectrum of this current is studied to obtain information about it. Depending on the sideband harmonics of the analyzed current, the type of fault can be predicted. Fast Fourier transform has been used to scan the frequencies and amplitudes, as well as the frequency spectrum, of stator line current [1–6].

3.3. Envelope of the Three-phase Stator Current

In addition to frequency analysis of stator current to detect the faults of induction machines, the envelope of the stator current is a helpful characteristic for fault classification. The stator current envelope of

the three-phase induction machine is used to identify the number of broken bars. The envelope signal is the change in amplitude for the stator currents due to fault occurrence. Therefore, the frequency of the envelope can be used as an indication to estimate the number broken bars.

Due to broken rotor bars, the envelope is generated in the stator currents. It is repeated regularly at a frequency given by:

$$f_{env} = 2Sf_s \tag{3}$$

4. MATHEMATICAL MODEL OF ELECTRICAL MACHINE USING MAXWELL'S EQUATIONS

Figure 1 shows the finite element model of the motor that has been used in simulation. The main formulas used in time stepping finite element analysis (TSFEA) are the Ampere law and conservation of flux density law [11, 12]:

$$\nabla \times \mathbf{H} = \mathbf{J} \tag{4}$$

$$\nabla \cdot \mathbf{B} = 0 \tag{5}$$

$$\nabla \times \mathbf{E} = -\frac{\partial \mathbf{B}}{\partial t} \tag{6}$$

where

H is the magnetic field intensity vector (A/m);

J is the current density vector (Amp/m^2);

B is the magnetic flux density vector (wb/m^2);

E is the electric field intensity vector (volt/m).

The above equation can be rewritten in terms of the magnetic vector potential **A** (web/m), where:

$$\mathbf{B} = \nabla \times \mathbf{A} \tag{7}$$

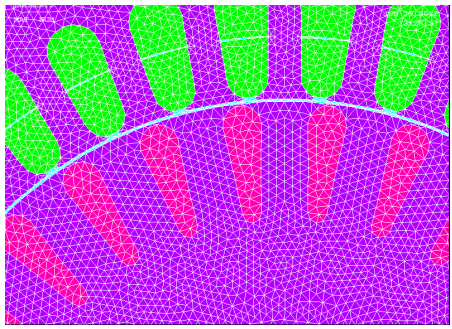

Figure 1. Finite element model of the motor section under simulation.

Substituting Eq. (7) in Eqs. (6) and (4) gives [13]:

$$\nabla \times \left(\frac{1}{\mu} \nabla \times \mathbf{A} \right) = \mathbf{J} \tag{8}$$

$$\nabla \left(\nabla \cdot \mathbf{A} \right) - \nabla^2 \mathbf{A} = \mu \mathbf{J} \tag{9}$$

μ is the magnetic permeability of the material.

Applying vector notation, where $\nabla(\nabla \cdot \mathbf{A}) = 0$, gives the Poisson equation:

$$\nabla^2 \mathbf{A} = -\mu \mathbf{J} \tag{10}$$

The current density ($\mathbf{J = 0}$) in the air-gap region, which gives the Laplace Equation as follows:

$$\nabla^2 \mathbf{A} = 0 \tag{11}$$

The power circuit elements have been coupled directly to the finite element region through coupling nodes [14]. ANSYS software provides a library of electrical elements (CIRCU124) for building the electric power circuit.

5. MODELING OF DEEP BAR INDUCTION MACHINE

5.1. Two-dimensional Assumptions for Finite Element Model

In order to reduce the simulation time without loss of the accuracy of the results, it is important to consider some assumptions for modeling process. A 2-D finite element method has been used to construct the geometry of the machine. For this modeling type, it is assumed that the current density $\mathbf{J}$ has only one component in z-direction, ($\mathbf{J}_z$), and can be written in the following form:

$$\mathbf{J} = (0, 0, \mathbf{J}_z) \tag{12}$$

The magnetic vector potential A has also one component ($\mathbf{A}_z$) in the same direction of $\mathbf{J}_z$, then:

$$\mathbf{A} = (0, 0, \mathbf{A}_z) \tag{13}$$

According to these assumptions, the magnetic flux density and magnetic flux intensity will have two components in the xy-plane ($\mathbf{B}_x$, $\mathbf{B}_y$, $\mathbf{H}_x$, $\mathbf{H}_y$) as given in the following equations, where $\mathbf{A}_z$ and $\mathbf{J}_z$ are perpendicular to this plane.

$$\mathbf{B} = (\mathbf{B}_x, \mathbf{B}_y, 0) \tag{14}$$

$$\mathbf{H} = (\mathbf{H}_x, \mathbf{H}_y, 0) \tag{15}$$

To simulate the materials of the stator slots regions, it is assumed that the stator windings consist of small cross sectional copper wires. Eq. (10) has been modified according to this assumption and may be rewrite in the following form:

$$-\frac{1}{\mu}\left(\frac{\partial^2 \mathbf{A}_z}{\partial x^2}+\frac{\partial^2 \mathbf{A}_z}{\partial y^2}\right)=\mathbf{J}_z \tag{16}$$

where, μ is the permeability of core material. In the air-gap region, the right hand term of Eq. (16) is equal to zero. Therefore, there is no induced current in this region.

For transient analysis, in addition to the previous assumptions, it has been assumed that the current density in the rotor region has a variable distribution over the rotor bars due to skin effect. Therefore, Eq. (16) can be modified to the following form:

$$\frac{\partial^2 \mathbf{A}_z}{\partial x^2}+\frac{\partial^2 \mathbf{A}_z}{\partial y^2}=-\left(\mu \mathbf{J}_z+\frac{\partial}{\partial t}\mu \mathbf{A}_z\right) \tag{17}$$

Eq. (17) is the governing equation that has been used to model the field distribution of the deep bar, three-phase induction motor with 2D finite element analysis model. The current density of Eq. (17) consists of two terms; the first is due to applied voltage on the stator winding while the other is the induced current in the conductor due to time variation of magnetic field.

5.2. Electric Circuit of Induction Motor

Stranded coils are used to simulate the effect of the induced emf in the stator windings. It is assumed that the stator winding of each coil consists of conductors with small cross section area. These conductors are grouped together to form the stranded coil. It is assumed that their contribution to the current density is averaged over the area of the winding. To represent a voltage fed device, circuit equations must be coupled with the field equations. Finite Elements Model (FEM) has been coupled directly to the supply circuit.

Since a 2-D finite element model has been used to assemble the geometry construction of the induction motor, the end winding and end ring parameters are not included in the model [15, 16]. The end parameters, especially end winding resistance, have a considerable effect on the dynamic performance of the motor at load conditions [17]. Thus, these parameters have been included in the external electric circuits, which are coupled directly with finite element domain [18].

For dynamic modeling of electrical motors using FEM, the electrical circuit and magnetic field domain should be coupled. In

this work, the electric circuit has been built by using ANSY circuit elements library.

5.3. Calculation of Developed Torque

The developed torque has been computed by means of Maxwell's stress tensor. For a 2-D finite element model, the stress tensor has been integrated along the middle of the air-gap l_g. Because of the numerical nature of the finite element method, the result may depend on both the position of the integrating line and the number of chosen nodes for the numerical integration. Then the torque is [19]:

$$T_e = \frac{l_s}{g\mu_o} P \int_{l_g} r B_r B_t \cdot ds \tag{18}$$

l_s is stack length (m);

g is the air-gap length (m);

P is the number of pole pairs;

r is the mean air-gap radius (m);

B_r is the radial component of the flux density (wb/m^2);

B_t is the tangential component of the flux density (wb/m^2).

The developed torque has been determined and used to calculate the angular speed on the rotor by solving the mechanical equation of rotation w_m. The dynamic equation of induction motor that couples between the electromagnetic torque and mechanical parameters is given by [20–22];

$$T_e = J\frac{dw_m}{dt} + Bw_m + T_L \tag{19}$$

where

T_e is the developed electromagnetic torque (N·m);

T_L is the steady-state load torque (N·m);

B is the viscous friction ((N·m)/rad/sec);

w_m is the mechanical rotor speed (rad/sec).

$$w_m = \frac{1}{P}\frac{d\theta_m}{dt} \tag{20}$$

θ_m is the angular position of the rotor (in electrical radius);

P is the number of pole pairs.

6. FAULTS DETECTION TECHNIQUES BASED ON FEM

Monitoring the operation of electrical machines is an important process for protecting this equipment from damages. Different parameters had been calculated to detect the faults on electrical machines. These calculations are based on the FEM in which the magnetic field variation is used to provide information about the stator and rotor currents, rotation and dynamic performance of the machine. In addition, FEM calculates the stored magnetic energy on the machine parts in order to predict the faults [23]. As a result, FEM is adopted in the present paper to determine the stator current, and then by using Fourier transform [24, 25] the frequency spectrum of the stator current is investigated. Depending on the sideband harmonics of the analyzed stator current, the type of fault has been predicted.

In the current research, three types of faults have been investigated. The first type is the broken rotor bars, which have been considered. As a result of this fault, the rotor bars current will reduce due to increasing the total impedance of the rotor bar circuit. Therefore, the rotor circuit will have an unbalanced operation, consequently the sideband components contained in the spectrum of the stator current. The frequency of these harmonics 'f_b' depends on a slip speed 'S' and stator current frequency 'f_s'. These sideband components are injected in the stator current.

The equation can be used to represent two sideband components in terms of frequency as follows:

$$f_b = f_s(1 \pm 2KS) \quad K = 1, 2, 3 \ldots . \tag{21}$$

The second type is the inter-turn short circuit on stator winding, which occurs due to aging, overloading or manufacturing. A short circuit may take place between some turns of stator coils of the same phase or with other two phases. The resultant stator MMF will be affected by this fault, and another harmonic component will be contained on stator current. The frequency 'f_{sc}' of sidebands due to inter-turn short circuit has been calculated using the relation [6]:

$$f_{sc} = \left\{ K \pm (1 - S)\frac{n}{P} \right\} f_s \tag{22}$$

where

f_{sc} is the short circuit frequency (Hz);

n is integer = 1, 2, 3, ..., $(2P - 1)$;

$K = 1, 3, 5, \ldots$.

The last type of faults is the air-gap eccentricity, which consists of three types, Static Eccentricity (SE), Dynamic Eccentricity (DE) and mixed Eccentricity (ME).

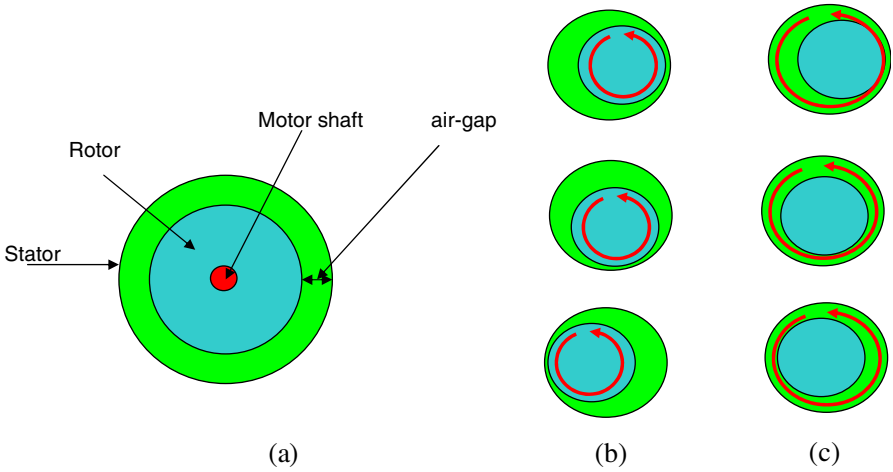

Figure 2. Geometry of induction motor, (a) healthy motor, (b) static eccentricity, (c) dynamic eccentricity.

It is a familiar rotor fault, which produces a pulsation in rotor speed of induction machine due to ripple torque. The noise and vibration are produced due to misalignment of the rotor along the geometric centre of the stator. These faults are due to the rotor deviation from the axial axis of the stator, deflection of rotor shaft, and movement of the stator frame. The air-gap eccentricity produces unbalance of radial forces which causes friction between stator and rotor windings. As a result, a damage of rotor bar and stator winding occurs. Figure 2 illustrates the rotation of rotor in the presence of air-gap eccentricity.

Under normal operation of the three-phase induction motor, the rotating magnetic field contains the fundamental components of the stator and rotor MMFs. Due to eccentricity fault, the resultant magnetic motive force (mmf) waveform is deviated, compared with normal condition, and the mmf space harmonic components are affected significantly. This will produce unbalanced distribution of the magnetic flux within the air gap. As a result, the rotating magnetic field in the air-gap consists of the fundamental components in addition to the harmonics components due to fault. The general formula of eccentricity components f_{ecc} in the stator current is given by [2, 8].

$$f_{ecc} = f_s \left[(KN_r \pm nd) \frac{(1-S)}{P} \pm \nu \right] \tag{23}$$

where

nd is the eccentricity order ($nd = 0$ for static eccentricity);

N_r is the number of rotor slots;

υ is the time harmonic of stator mmf = 1, 3, 5, ...;

K is any integer ($K = 1, 2, 3, \ldots$).

The amplitude of harmonics components depends on the type and degree of the eccentricity. In the case of static eccentricity, the frequency (f_{ecc}) of the harmonic components is given by:

$$f_{ecc} = f_s \left[(KN_r) \frac{(1-S)}{P} \pm \nu \right] \tag{24}$$

7. MODELING OF CAGE TYPE INDUCTION MOTOR

The first step for fault diagnosis process is to construct a model, which gives an accurate representation of the electrical machine. Mechanical elements of the machine as well as the coupling equations of the electromagnetic device should be included in the proposed model. Three main conventional methods had been used for machine modeling in the field of fault diagnosis. The magnetic coupling method (MCM), Winding Function Method (WFM), Extended Winding Function Method (EWFM) and finite element method (FEM) had been used to simulate the induction motor under healthy and faulty conditions [26–28]. The classical methods of modeling and simulation are simple, easy to manipulate and give approximate results because they are based on approximation criteria. The basic equations of these techniques, in case of uniform air-gap, are different for non-uniform air-gap. Also the electrical machine is assumed to work in linear region where the effect of saturation is not considered.

In the FEM, the magnetic field distribution, non-linearity of core materials and saturation effects are taken into consideration. Therefore, faults detection based on magnetic property variation can be taken into account. In the present work, a Time Stepping Finite Element Analysis (TSFEA) has been used to model the healthy and faulty motor. This method is used to calculate the magnetic field distribution within the different parts of the machine to obtain the actual values of stator currents, power loss, magnetic energy, speed and dynamic torque [29–32].

8. MODELING OF INDUCTION MOTOR UNDER FAULT CONDITIONS

Finite element method offers special ability to model and study the faults occurring in electrical machines. It provides a way to study the

performance, supervise and diagnosis different types of faults. FEM provides a simulation condition that can be used to control all the external environments as well as the structure of the electric machine.

Considering the modeling of cage rotor type three-phase induction motor, three types of faults, broken-bars, inter-turn short circuit of stator winding and air-gap eccentricity have been modeled using ANSYS software. The modeling procedure that has been followed to form these faults can be explained as follows.

In the first type of fault, the broken bars of the rotor are modeled with high resistivity material, and as a result, very low current actually will still pass through the faulty bar. Lost current in the electrical circuit of the rotor will produce unbalance currents in the other circuit branches; as a result, the magnetic flux and magnetic flux density in the air-gap region will be distorted. This distortion will inject sideband harmonics with the fundamental MMF component. The effect of these harmonics will be transferred to the stator current, which will also contain harmonics due to this fault. The value of the low frequency current harmonics can be calculated using Eq. (21). The amplitude of the harmonics depends on the slip speed of the motor and the number of broken bars.

In the second type of faults, short circuit in stator winding may occur due to the damage in the insulator of stator winding, bent of the rotor or negative sequence current. To simulate the short circuit fault on stator winding, it is necessary to reduce the winding number of the coils. ANSYS software provides a command (rmodif) for modifying the number of winding for each stator slot. As a result, a direct modeling has been implemented to simulate the faults between two turns or coils, single phasing and line-to-line. The order of harmonic components of the stator currents have been detected based on Eq. (22). Early detection of this fault could reduce the maintenance requirements as well as increase the lifetime of the motor. The amplitudes of harmonic components, which can be predicted by using FEM, give an indication to the winding fault conditions.

The third type of fault is air-gap eccentricity, which can be produced due to manufacturing or due to unbalance forces on the rotor by external torques on the rotor shaft. The usual method for detecting this type of faults is based on monitor the current signature of stator current. Two parameters give a significant effect on this type of fault: the frequency of the produced harmonics and the amplitude of these components. Eq. (24) has been used to detect the harmonics order due to this fault. A dynamic eccentricity using FEM has been modeled by changing the axial axis of rotor from coincidence with both stator and rotor rotation axes of the machine. The mixed faults

of induction motor have also been included and analyzed in this work. Mixed faults prediction includes static eccentricity with two broken bars, static eccentricity with four broken bars, static eccentricity and 10% inter turn short circuit of stator winding.

9. SIMULATION RESULTS

A three-phase, cage rotor type, 4-pole, 36-stator slot, double-layer, 28-rotor bar, induction machine has been used in the present simulation. The parameters of the 3-phase, 380 V, Y-connection, 18.5 kW induction motor are given in Table 1. A 2-D, transient analysis has been used to solve a set of Maxwell's equations based on FEM. The magnetic fields over the model have been calculated, and as a result, all stator and rotor parameters have been obtained. The time variations of stator current at no-load and rated load under healthy condition are explained in Figures 3(a), (b). The frequency spectrum of stator line current for healthy motor is shown in Figure 4.

In addition, simulated results for faulty motor are presented, which consider both singular and multi-faults in the following sections.

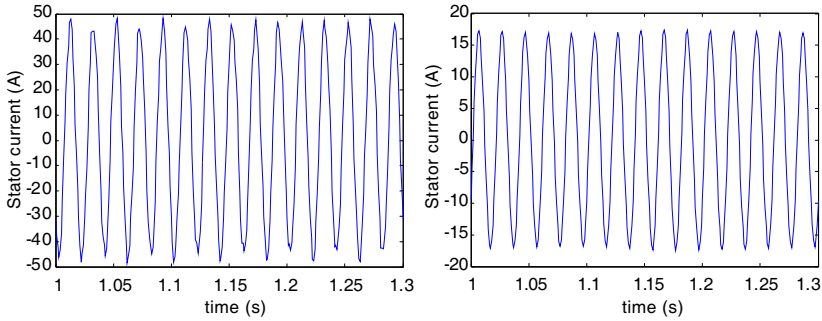

Figure 3. Time variation of stator current under steady state condition, (a) load condition, (b) no-load condition.

Table 1. Data of the induction machine used in the simulation.

Rated voltage	380 V-Y	Outer radius of stator	135 mm
Output power	18.5 kw	Outer radius of rotor	88.4 mm
Pair pole	2	Stack length	180 mm
Rated speed	1460 rpm	Connection	Star
Supply frequency	50 Hz	Rated torque	100 Nm
Rated supply current	35 A-Y		

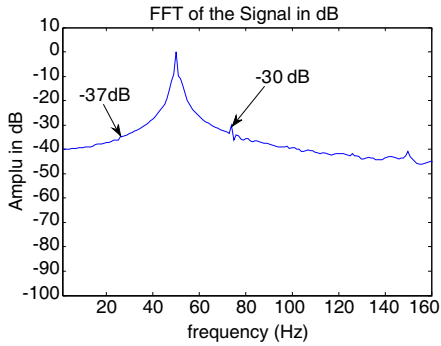

Figure 4. Frequency spectrum of stator current for healthy motor under load condition.

9.1. Separated Faults

9.1.1. Broken Rotor Bar Results

The resistivity of rotor bars in the case of faulty motor has been assumed to have a high value. Fast Fourier transform has been used to determine the frequency and amplitude of the frequency spectrum of stator line current. The time variations of stator current for two and four broken bars are shown in Figure 5.

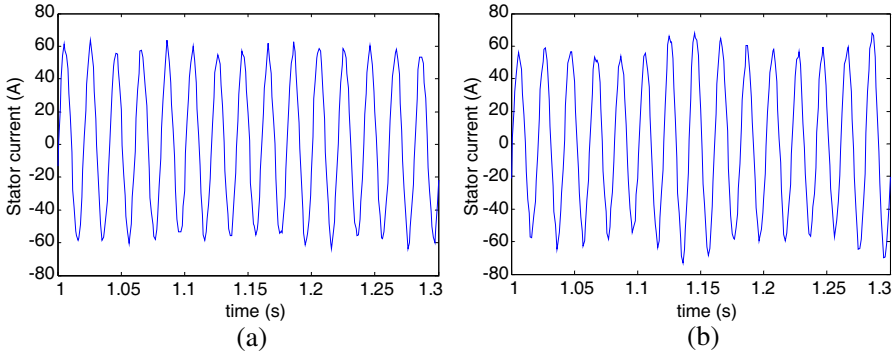

Figure 5. The stator current, (a) 2-broken bar condition, (b) 4-broken bar condition.

The stator line current at rotor speed 1440 rpm has a ripple shape due to fault. The increasing number of broken bars leads to increasing the severity of ripple. The frequency spectrum for this fault has a two side-band harmonic according to Eq. (21) as explained in Figure 6. The left component LSH is on 44.05 Hz, while the right one RSH is on 55.55 Hz for two broken bars. In the second case, for four broken bars, the left and right components are on 44.48 Hz and 57.56 Hz,

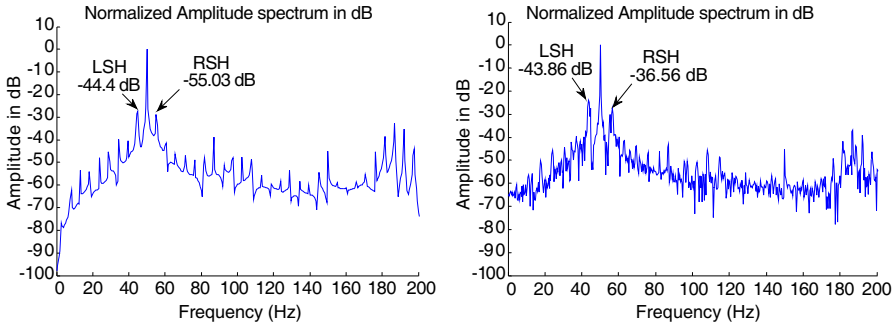

Figure 6. The frequency spectrum of stator current for (a) 2-broken bar condition, (b) 4-broken bar condition.

Table 2. The amplitude and frequency variation under broken bars faults.

	Rotor speed (rpm)	LSH (dB)	Frequency (Hz)	RSH (dB)	Frequency (Hz)
Two broken Bar	1440	−26.56	44.05	−28.5	55.55
Four broken Bar	1420	−23.77	44.48	−27.74	57.56

Table 3. The frequency comparison between FEM and analytical results.

No. of Broken Bars	Motor Speed (rpm)	slip	RLSH (Hz)		RSH (Hz)	
			FEM	Analytic Formula	FEM	Analytic Formula
Two broken bars	1423	0.05133	44.05	44.866	55.55	55.133
Four broken bars	1391	0.07266	42.48	42.7333	57.56	57.266

respectively. The amplitude and frequency of the sidebands harmonics components are given in Table 2.

To validate the simulation, a comparison between the results obtained from finite element solution and analytical formula in Eq. (21) is illustrates in Table 3.

9.1.2. Stator Short Circuit Windings

Stator slots of the motor have a double coil on each slot. In the present work, a short circuit has been assumed between two adjacent coils referred to the same phase. Since the number of stator windings due to fault is reduced, the stator current will increase. Consequently, two harmonics components will appear on the frequency spectrum of stator current. The value of these sidebands can be calculated using Eq. (22). This type of faults will produce unbalance on the number of winding with respect to other phases. As a result, the amplitude of sideband harmonics components is increased. Figures 7 and 8 present the results, stator current and its spectrum, for 30% and 15% of inter turn short circuit fault respectively.

The other healthy phases stator currents are slightly affected. The

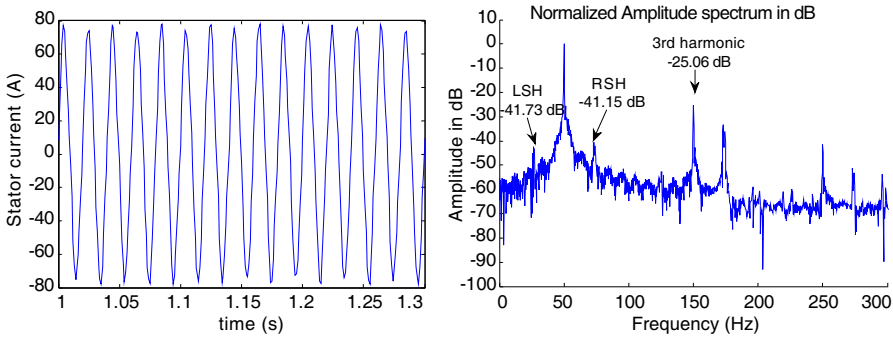

Figure 7. The inter-turn short circuit (30%) condition, (a) time variation, (b) frequency spectrum.

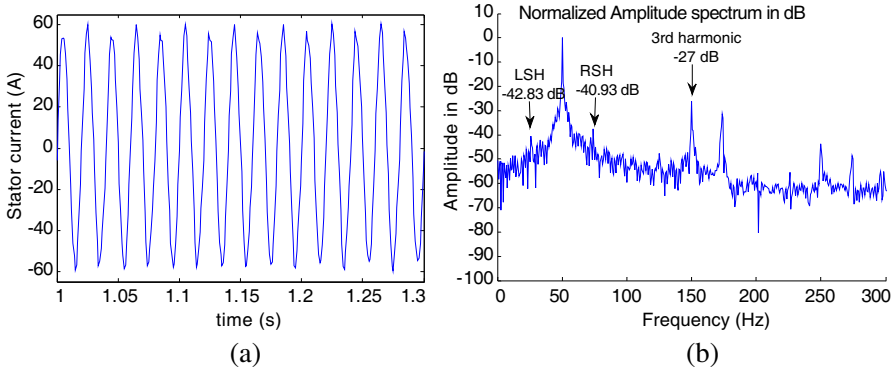

Figure 8. The inter-turn short circuit (15%) condition, (a) the time variation, (b) the frequency spectrum.

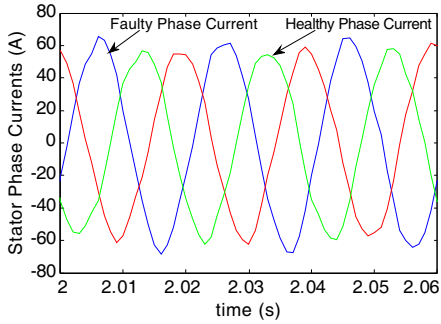

Figure 9. Three-phase stator current of the induction motor with inter-turn short circuits on one phase under full load condition.

three-phase stator currents for the induction motor with inter-turn short-circuit are shown in Figure 9.

9.1.3. Air-gap Eccentricity

Figure 10 illustrates the frequency and time variation of the stator line current under the consideration of 33.33% static air-gap eccentricity. From Eq. (24), the spectrum of the line current will have two harmonics. The amplitude value of the stator line current will not vary and equal to its value on healthy operation.

Table 4 illustrates a comparison between the results obtained from finite element solution and analytical formula in Eq. (24).

Figures 11 and 12 show the waveforms of stator current in the case of two and four broken bars, respectively. It is clear from the

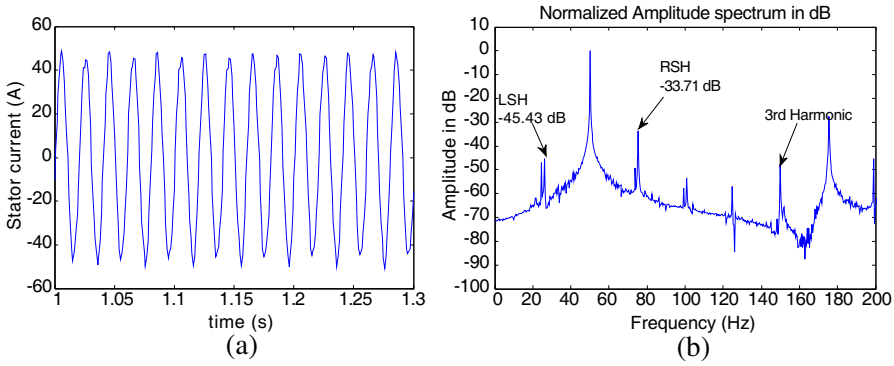

Figure 10. The stator line current under air-gap eccentricity condition, (a) the time variation, (b) the frequency spectrum.

Table 4. A comparison between finite element solution and analytical formula results in case of air-gap eccentricity fault.

Motor Speed (rpm)	slip	LSH (Hz)		RSH (Hz)	
		FEM	Analytic Formula	FEM	Analytic Formula
1447	0.035333	26.14	25.88	75.36	74.6

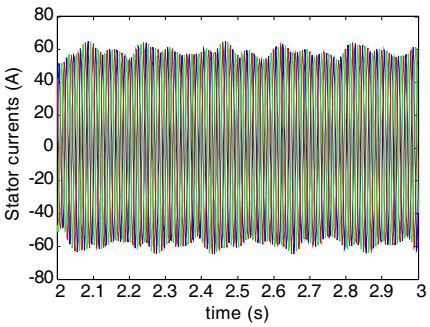

Figure 11. The stator current envelope-two broken bars under rated load.

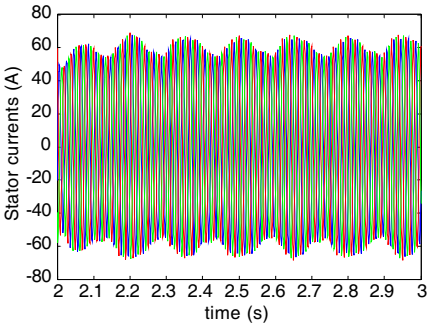

Figure 12. The stator current envelope-four broken bars under rated load.

figures that the envelope of the three-phase stator currents is generated and causes a change to the general shape of the currents. The envelope is repeated periodically at a frequency equal to 2 Sf. The frequency and amplitude of the envelope are directly proportional to the number of broken bars. Increasing the number of broken bars leads to increasing the angular deflection for the magnetic axis of rotating mmf. Consequently, the magnetic field of the stator is distorted and modulates in a sequential manner.

10. MIXED FAULTS

Figures 13 and 14 show the frequency components of the stator current air-gap eccentricity with two and four broken bars, respectively. The harmonic components due to broken bars appear at $f_s(1 \pm KS)$. In addition, two side-band components due to static eccentricity are located on f_{ecc}.

Figure 15 shows the frequency spectrum of stator current in the case of air-gap eccentricity and inter-turn short circuit of stator winding. These types of faults produce side-band components at the

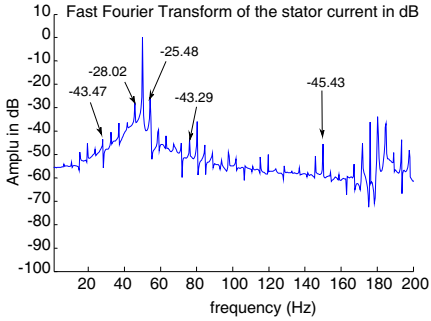

Figure 13. The stator line current under air-gap eccentricity with two broken bars condition.

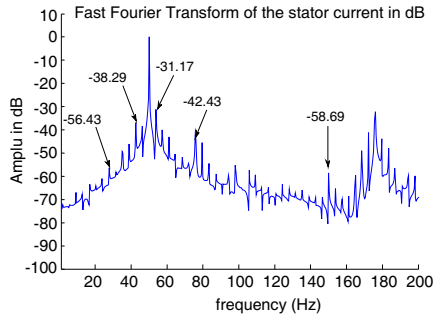

Figure 14. The stator line current under air-gap eccentricity with four broken bars condition.

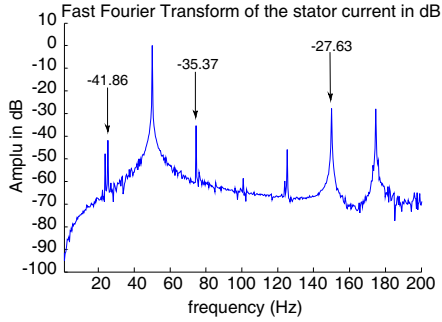

Figure 15. The stator line current under air-gap eccentricity with 10% stator winding short circuit condition.

Table 5. Amplitude and frequency variation under faults conditions.

	LSH		RSH		Sideband Harmonic ($k = 4$)	
	dB	Hz	dB	Hz	dB	Hz
Stator short circuit (15%)	−42.83	25.9	−40.93	74	−27	149.9
Stator short circuit (30%)	−42.73	26.73	−40.75	74.6	−25.06	149.9
Air-gap eccentricity	−49.36	26.14	−37.32	75.36	−46	149.9

same location (Eqs. (22) and (24)). The amplitude of the frequency component at $f_s = 149.9\,\text{Hz}$ is grater than the fault with eccentricity or short circuit of stator winding.

11. DISCUSSION AND CONCLUSION

Finite element method provides a representation of complex geometry of the electrical machines as well as the actual non-linearity and saturation of the core materials. As a result, this method will reduce the cost and effort for damaging a real machine.

It is clear from simulation results that the amplitude of sidebands harmonics components will increase when the number of broken bars is increased as shown in Figure 2 and Figure 3. In addition, the shape of stator currents is detoured from sinusoidal waveform and has a ripple nature due to the effect of the distorted rotor MMF. The value of ripple is increased as the number of broken bars is increased.

Based on the rules for calculating the harmonics produced in stator line currents generated in the air-gap eccentricity and inter-turn short circuit, there are two sidebands components in the spectrum on (74 and 26) Hz. The harmonic component depends on the degree of each fault type. In order to distinguish between the two fault types, it is necessary to compare the amplitude of the stator current in time domain. In the case of short circuit fault, the stator current will have a high value compared with air-gap eccentricity.

It is clear from the frequency spectrum that the sideband harmonics components have greater values in the case of short circuit due to unbalance situation in the three-phase circuit of the stator winding. In the case of air-gap eccentricity, the unbalance rotor mmf will inject a side-band harmonic in the balance stator currents. Due to the inter-turn short circuit, the rotating mmf produced by unbalanced stator currents will also be unbalanced and affect the shape of rotor mmf. Then the unbalanced rotor mmf will inject a side-band harmonic in the unbalanced stator current. Therefore, the amplitude of the side band harmonic in this case has a greater value than the air-gap eccentricity.

Table 5 shows the amplitudes of left and right sideband harmonics under different faults conditions. The value of harmonic component may give an exact indication about the type of fault more than the frequency value. Due to broken rotor bars, the magnetic neutral axis of magneto motive force shifts from the normal location in the case of healthy motor. This deviation produces a shift in the angular position and waveform distortion of the rotor mmf. This variation is a function of the location as well as the number of broken bars.

REFERENCES

1. Faiz, J., B. M. Ebrahimi, B. Akin, and H. A. Toliyat, "Finite-element transient analysis of induction motors under mixed eccentricity fault," *IEEE Transactions on Magnetic*, Vol. 44, 66–74, 2008.
2. Faiz, J., B. M. Ebrahimi, B. Akin, and H. A. Toliyat, "Comprehensive eccentricity fault diagnosis in induction motors using finite element method," *IEEE Transactions on Magnetic*, Vol. 45, 1764–1767, 2009.
3. Faiz, J., B. M. Ebrahimi, and M. B. B. Sharifian, "Finite element transient analysis of an on-load three-phase squirrel-cage induction motor with static eccentricity," *IEEE Transactions on Magnetic*, Vol. 44, 207–227, 2007.
4. Akin, B., U. Orguner, H. A. Toliyat, and M. Rayner, "Low order PWM inverter harmonics contributions to the inverter-fed induction machine fault diagnosis," *IEEE Transactions on Industrial Electronics*, Vol. 55, 210–219, 2008.
5. Abdesselam, L. S., M. Ammar, and C. Guy, "Analysis of inter-turn short circuit in slots by finite element model," *IEEE 10th International Conference on Environment and Electrical Engineering (EEEIC)*, 1–4, Rome, Italy, May 8–11, 2011.
6. Verucchi, C. J., G. G. Acosta, and F. A. Benger, "A review on fault diagnosis of induction machines," *Latin American Applied Research*, 113–121, 2008.
7. Toliyat, H. A., M. S. Arefen, and A. G. Parlos, "A method for dynamic simulation of air-gap eccentricity in induction machines," *IEEE Transactions on Industry Applications*, Vol. 32, 910–918, 1996.
8. Nandi, S., R. M. Bharadwaj, and H. A. Toliyat, "Performance analysis of a three-phase induction motor under mixed eccentricity condition," *IEEE Trans. Energy Conv.*, Vol. 17, 392–397, 2002.
9. Nagarajan, S. and R. S. Rama, "Detection of inter-turn fault in three phase squirrel cage induction motor using finite element method," *European Journal of Scientific Research*, Vol. 58, 384–391, 2011.
10. Aileen, C. J., S. Nagarajan, and R. S. Rama, "Detection of broken bars in three phase squirrel cage induction motor using finite element method," *IEEE 2011 International Conference on Emerging Trends in Electrical and Computer Technology (ICETECT)*, 249–254, Tamil Nadu, India, Mar. 23–24, 2011.
11. Wang, X. and D. Xie, "Analysis of induction motor using field-

circuit coupled time-periodic finite element method taking account of hysteresis," *IEEE Transactions on Magnetic*, Vol. 45, 1740–1743, 2009.

12. Nicola, B., *Electrical Machine Analysis Using Finite Elements*, 1st Edition, Taylor & Francis Group, USA, 2005.
13. Sarac, V. and G. Stefanov, "Calculation of electromagnetic fields in electrical machines using finite elements method," *International Journal of Engineering and Industries*, Vol. 2, 1–29, 2011.
14. Gmiden, M. H. and H. Trabelsi, "Calculation of two-axis induction motor model using finite elements with coupled circuit," *IEEE 6th International Multi-conference on Systems, Signals and Devices (SSD'09)*, 1–6, Djerba, North Africa, Mar. 23–26, 2009.
15. De Weerdt, R. and E. Tuinman, "Finite element analysis of steady state behavior of squirrel cage induction motors compared with measurements," *IEEE Transactions on Magnetics*, Vol. 33, No. 2, 2093–2096, Mar. 1997.
16. Silwal, B. and A. Arkkio, "Computation of eddy currents in a solid rotor induction machine with 2-D and 3-D FEM," Master Thesis, Aalto University, 2012.
17. Islam, M. J., "Finite-element analysis of eddy currents in the form-wound multi-conductor windings of electrical machines," Doctoral Dissertation, Helsinki University of Technology, 2011.
18. Fu, W. N., P. Zhou, D. Lin, S. Stanton, and Z. J. Cendes, "Modeling of solid conductors in two-dimensional transient finite-element analysis and its application to electric machines," *IEEE Transactions on Magnetic*, Vol. 40, No. 2, Mar. 2004.
19. Yang, T., L. Zhou, and L. Li, "Parameters and performance calculation of induction motor by nonlinear circuit-coupled finite element analysis," *IEEE Trans. Power Electronics and Drive Systems, PEDS 2009*, 979–984, 2009.
20. Lin, R. and A. Arkkio, "Calculation and analysis of stator end-winding leakage inductance of an induction machine," *IEEE Transactions on Magnetic*, Vol. 45, No. 4, Apr. 2009.
21. Aroui, T., Y. Koubaa, and A. Toumi, "Modeling of cage induction machines: Application to diagnosis," *Third International Conference on Systems, Signals & Devices*, Sousse, Tunisia, Mar. 21–24, 2005.
22. Aroui, T., Y. Koubaa, and A. Toumi, "Magnetic coupled circuits modeling of induction machines oriented to diagnostics," *Leonardo Journal of Sciences*, No. 13, 103–121, ISSN 1583-0233, Jul.–Dec. 2008,

23. Ying, X., "Characteristic performance analysis of squirrel cage induction motor with broken bars," *IEEE Transactions on Magnetics*, Vol. 45, No. 2, 759–766, 2009.
24. Faiz, J. and B. M. Ebrahimi, "Mixed fault diagnosis in three phase squirrel-cage induction motor using analysis of air-gap magnetic field," *Progress In Electromagnetic Research*, 239–255, 2006.
25. Mirafzal, B. and N. A. O. Demerdash, "Induction machine broken-bar fault diagnosis using the rotor magnetic field space-vector orientation," *IEEE Trans. Ind. Appl.*, Vol. 40, 534–542, 2004.
26. Mirafzal, B. and N. A. O. Demerdash, "Effects of load magnitude on diagnosing broken bar faults in induction motors using the pendulous oscillation of the rotor magnetic field orientation," *IEEE Trans. Ind. Appl.*, Vol. 41, 771–783, 2005.
27. Faiz, J. and I. Tabatabaei, "Extension of winding function theory for non-uniform air gap in electric machinery," *IEEE Transactions on Magnetics*, Vol. 38, 3654–3657, 2002.
28. Faiz, J., I. Tabatabaei, and H. A. Toliyat, "An evaluation of inductances of a squirrel-cage induction motor under mixed eccentric conditions," *IEEE Trans. Energy Convers.*, Vol. 18, 252–258, 2003.
29. Tabatabaei, I., J. Faiz, H. Lesani, and M. T. Nabavi-Razavi, "Modeling and simulation of a salient-pole synchronous generator with dynamic eccentricity using modified winding function theory," *IEEE Transactions on Magnetic*, Vol. 40, 1550–1555, 2004.
30. Ebrahimi, B. M., J. Faiz, S. Lotfi-Fard, and P. Pillay, "Novel indices for broken rotor bars fault diagnosis in induction motors using wavelet transform," *ELSVIER Mechanical Systems and Signal Processing*, Vol. 30, 131–145, 2012.
31. Akar, M. and C. I. Ankaya, "Broken rotor bar fault detection in inverter-fed squirrel cage induction motors using stator current analysis and fuzzy logic," *Turk. Journal Elec. Eng. & Comp. Sci.*, Vol. 20, 1077–1089, 2012.
32. Li, W., Y. Xie, J. Shen, and Y. Luo, "Finite element analysis of field distribution and characteristic performance of squirrel-cage induction motor with broken bars," *IEEE Transactions on Magnetics*, Vol. 43, 1537–1540, Apr. 2007.